A Calculation Model of Charge and Discharge Capacity of Electric Vehicle Cluster Based on Trip Chain

HAIFENG LIANG[1], **(Member, IEEE), ZIYANG LEE**[1], **AND GEN LI**[2], **(Member, IEEE)**

[1]Department of Electrical Engineering, North China Electric Power University, Baoding 071003, China
[2]School of Engineering, Cardiff University, Cardiff CF24 3AA, U.K.

Corresponding author: Haifeng Liang (hfliang@ncepu.edu.cn)

ABSTRACT The rapid response characteristics and high-speed growth of electric vehicles (EVs) demonstrate its potential to provide auxiliary frequency regulation services for independent system operators through vehicle-to-grid (V2G). However, due to the spatiotemporal random dynamics of travel behavior, it is challenging to evaluate the ability of EV cluster to provide ancillary services under the premise of reaching the expected state of charge (SOC) level. To address this issue, a novel calculation model of charge and discharge capacity of EV cluster based on trip chain with excellent parallel computing performance is presented in this work. Following the introduction of the characteristic variables of the proposed trip chain model, the user's continuous travel behavior in a time scale of several weeks is simulated. In particular, a bidirectional V2G scheduling strategy based on the five-zone map is designed to guide the charging and discharging behavior of EVs, where the expected SOC levels are guaranteed. The results of a 3-week travel simulation verify the effectiveness of the presented model in coordinating the V2G scheme and calculating the charge and discharge capacity of the EV cluster.

INDEX TERMS Charge and discharge capacity, electric vehicles, expectation-maximization, trip chain, vehicle-to-grid.

I. INTRODUCTION

In recent years, the development of renewable energy sources, such as wind and solar power, has made great progresses. By the end of 2018, China's full-caliber power generation capacity has reached to 1900GW, including 184.27GW of wind power and 174.33GW of solar power with increases of 12.4% and 33.7% over the previous year, respectively. The proportion of renewable energy installed has reached 18.9%. The strong intermittence of renewable energy sources may lead to inevitable frequency variations, while conventional generating units cannot provide frequency regulation services in a cost-effective manner [1]–[3]. Meanwhile, as an environment-friendly alternative to internal combustion engine vehicles, electric vehicles (EVs) have been widely promoted around the world. By 2030, the number of EVs in China will reach 60 million with a power

The associate editor coordinating the review of this manuscript and approving it for publication was Guangya Yang.

consumption of about 1.3% of the national electricity consumption. The peak charging load will reach to 479GW, while uncoordinated charging may result in energy losses, voltage deviations, transformer overload, and electricity prices increasing [4]–[7].

New methods to model EV charging loads are under development. By assuming that the user's initial states of charge (SOC) follows a certain normal distribution, references [8] and [9] use the method of Monte Carlo to draw samples of the arrival time, driving mileage, and the initial SOC of EVs to calculate the daily charging load profiles. However, the conditions of using this method may be too strict to fully reflect the randomness of user travel patterns. The queuing models for calculating the load of the charging station are proposed in [10] and [11] based on the assumption that the arrival time of EVs at the charging station follows the Poisson Distribution. This method is suitable for calculating charging loads in centralized places such as shopping mall car park, highway service areas, etc. However, the effectiveness

of this model to calculate decentralized charging loads needs to be improved. By considering the impact of economics, convenience, and driving preferences on the charging behavior of EVs, an agent-based simulation model is proposed in [12] and [13] to evaluate the impact of EV charging on grid loads. In order to describe the spatial-temporal randomness of the user's travel behavior, the trip chain theory based on the Markov Random Process is used in [14]–[18]. By fitting the user's travel characteristics on weekdays and weekends such as the departure time, driving distance, and parking duration, the charging loads under different parking scenarios are calculated in [17]. An inhomogeneous Markov model is presented in [18] to capture the diurnal variation in the use of an EV, where a large number of parameters are reduced by using B-spline. However, the complexity of the model may limit its applications in scenarios with large-scale EVs.

EV cluster is a collection of a large number of EVs in a certain area. By controlling the charging and discharging behavior of EV clusters to track Automatic Generation Control (AGC) signals, vehicle-to-grid (V2G) could provide ancillary services such as frequency regulation and voltage regulation, even reducing wind and photovoltaic active power curtailment. According to the studies in [2], [19]–[26], the V2G control strategies could be broadly classified into two main categories: unidirectional V2G and bidirectional V2G.

Unidirectional V2G is technically easy to be implemented, through which power can only flow from the grid to the EV [2], [19]–[20]. A unidirectional V2G hierarchical model that satisfies both supplementary frequency regulation and user travel needs is presented in [2], which allocates AGC signals based on the EV's regulation capability. However, this model is similar to the one presented in [19], wherein the V2G power of each EV is determined by the charging station, which makes it unsuitable for decentralized charging scenarios. A V2G model for frequency regulation under the performance-based compensation scheme is proposed in [20], which maximizes the user's income by improving the EV's ability to track AGC signals. However, this scheme fails to consider the impact of frequency regulation on battery losses.

Bidirectional V2G requires higher requirements on the inversion performance of charging equipment, which achieves a bidirectional power flow between the EV battery and grid [21]–[26]. A two-level hierarchical control mechanism based on mixed-integer linear programming is proposed in [21]. The EV charging and discharging scheme is determined by estimating the EV frequency modulation capability of the charging station and substation in each time slot. The capability of EVs in executing the reactive power compensation by tracking AGC signals is investigated in [22]. V2G-based EV supplementary frequency regulation has been adopted by many Independent System Operators (ISOs), such as PJM, California ISO, New York ISO and Midcontinent ISO [20]. However, the method of obtaining the intuitive charging and discharging capabilities of EV clusters is still under-researched.

To overcome these issues and maximize the contribution of bidirectional V2G to the grid, two major challenges still exist as follows:

1) The primary purpose of EVs is to meet users' travel needs. Therefore, based on practical data, analyzing the user's travel pattern through the trip chain model with time-space variation probability is the fundamental work to study the impact of integrating large-scale EVs on power grids.

2) Evaluating the ability of large-scale EV clusters to respond to AGC signals, i.e. charge and discharge capacity, on the premise of obtaining the expected battery SOC level, helps to guide the mid- and long-term planning of power grids and the assessment of renewable energy consumption capacity.

The contributions of this article include:

1) Based on the spatiotemporal-varying probabilistic characteristics of starting and ending a trip, the probability distributions of the trip chain characteristic variables are fitted.

2) The trip chains on a time scale of several weeks of the EV clusters are simulated, which can reflect the spatial-temporal distribution of EVs' diurnal driving patterns. Moreover, the simplified block structure makes it more suitable for the simulation of large-scale EV cluster travel behavior than the method presented in [18].

3) Inspired by the nine-zone map model applied in the control of substation voltage and reactive power [27], [28], a five-zone map model with closed boundaries is proposed, which is a new tool to describe the ability of an EV to respond to AGC signals more intuitively than the methods in [20], [21], [23] under the premise of meeting the owner's travel needs.

4) The charge and discharge capacities of the EV cluster are calculated based on the trip chains and the five-zone map.

5) The simulation of travel and charge-discharge behaviors are parallelized to increase the calculation speed based on the consideration that the EVs in the cluster are independent of each other.

The rest of this article is organized as follows. Section II introduces the modeling of trip chains. Section III provides the mathematical model of the five-zone map. Section IV illustrates the calculation process. Section V presents the details of the proposed model and the results of a case study. The conclusion drawn from the study is provided in Section VI.

II. TRIP CHAIN THEORY
A. STRUCTURE OF THE TRIP CHAIN

Analyzing the EV user's travel pattern with time-space variation probability is the fundamental work to study the charging demand of EVs. The trip chain model can be used to reflect the dynamic characteristics of the travel pattern. A trip chain model is proposed based on the related studies in [15], [17], [18], [29]–[31], its structure is illustrated in Figure 1. B_i is the i-th trip block in the trip chain, $T_{s,i}$, $T_{a,i}$, and $T_{g,i}$ are the departure time, arrival time, and parking end time
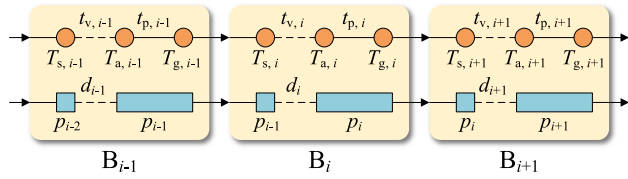
FIGURE 1. Structure of a trip chain.

of the i-th trip, $t_{v,i}$ and $t_{p,i}$ are the driving time and parking duration of the i-th trip, p_{i-1} and p_i are the departure type and destination type of the i-th trip, d_i is the driving mileage of the i-th trip.
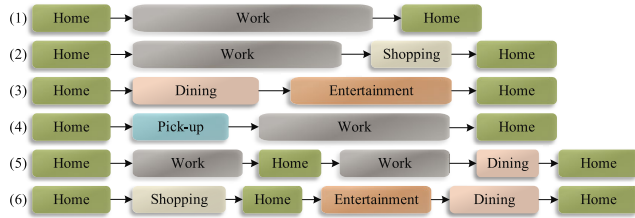

FIGURE 2. Examples of typical trip chains.

Six typical trip chains composed of daily activities are shown in Figure 2. Some references limit the length of the trip chain, for instance, by reducing the number of trips in one day [15], [16]. In order to fully consider the randomness and continuity and explore the diversity of travel laws on a long timescale, this article does not reduce the length of the trip chain and does not force EVs to return home at the end of the day during the simulation.

The U.S. Federal Highway Administration released the latest National Household Travel Survey (NHTS) in 2017. It is assumed that EV owners have the same travel patterns as the survey, hence the TRIPPUB.csv file released in the survey is used as the dataset in this article.

B. CHARACTERISTIC VARIABLES OF THE TRIP CHAIN

Each trip in the trip chain is abstracted into a trip block consists of several characteristic variables that follow different distributions. The fitting methods of the characteristic variables are described as follows:

1) THE FIRST DEPARTURE TIME OF A DAY

The frequency histogram of the first departure time of a day is shown in Figure 3. It shows that the first departure time follows a Gaussian mixture distribution. Therefore, the Expectation-Maximization (EM) algorithm in [32] is used to fit the parameters of the Gaussian mixture distribution.

According to the probability theory, the probability density function (PDF) $p(x)$ of a one-dimensional Gaussian mixture distribution array $X = \{x_1, x_2, \ldots, x_N\}$ can be expressed as:

$$
\begin{cases}
p(x|\Theta) = \sum\limits_{k=1}^{M} \omega_k p_k (x|\theta_k) \\
p_k (x|\theta_k) = \dfrac{1}{\sqrt{2\pi\sigma_k^2}} \exp\left[-\dfrac{(x-\mu_k)^2}{2\sigma_k^2} \right]
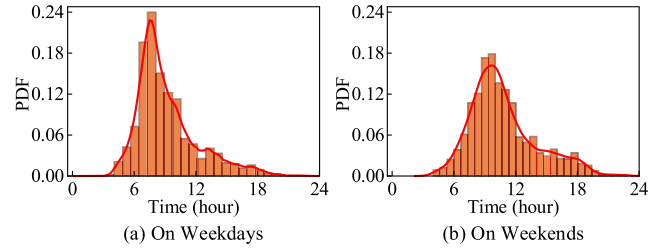\end{cases}, \quad (1)
$$

FIGURE 3. PDF histograms of the daily first departure time.

where $\Theta = (\omega_1, \omega_2, \ldots, \omega_M, \theta_1, \theta_2, \ldots, \theta_M)$ indicates that the Gaussian mixture distribution is composed of a finite number of M single Gaussian distributions, ω_k is the weight of the k-th single Gaussian distribution, which satisfies $\sum_{k=1}^{M} \omega_k = 1$, θ_k is the mean and standard deviation (μ_k, σ_k) of the k-th single Gaussian distribution, $p_k(x|\theta_k)$ is the PDF of the k-th single Gaussian distribution.

For simplicity, the readers are referred to the proof of parameter-estimation of Gaussian mixture distribution based on the EM algorithm in Appendix A. The steps to use the EM algorithm are given in (2)-(4).

According to the Bayesian theory, the probability that the i-th sample x_i is generated by the k-th Gaussian distribution is:

$$
p\left(k|x_i, \Theta^{(t)}\right) = \frac{p\left(k, x_i|\theta_k^{(t)}\right)}{p\left(x_i|\Theta^{(t)}\right)} = \frac{\omega_k p_k \left(x_i|\theta_k^{(t)}\right)}{\sum_{j=1}^{M} \omega_j p_j \left(x_i|\theta_j^{(t)}\right)}, \quad (2)
$$

where $\Theta^{(t)}$ is the estimated value of Θ at the beginning of the t-th iteration.

The distribution parameter $\Theta_k^{(t+1)} = (\omega_k^{(t+1)}, \mu_k^{(t+1)}, \sigma_k^{(t+1)})$ of each Gaussian distribution is calculated iteratively:

$$
\begin{cases}
\omega_k^{(t+1)} = \dfrac{\sum_{i=1}^{N} p\left(k|x_i, \Theta^{(t)}\right)}{N} \\
\mu_k^{(t+1)} = \dfrac{\sum_{i=1}^{N} \left[x_i p\left(k|x_i, \Theta^{(t)}\right)\right]}{\sum_{i=1}^{N} p\left(k|x_i, \Theta^{(t)}\right)}, \forall k \in \{1, 2, \cdots, M\} \\
\left(\sigma_k^2\right)^{(t+1)} = \dfrac{\sum_{i=1}^{N} \left[(x_i - \mu_k)^2 p\left(k|x_i, \Theta^{(t)}\right)\right]}{\sum_{i=1}^{N} \left[p\left(k|x_i, \Theta^{(t)}\right)\right]}
\end{cases}, \quad (3)
$$

The iteration ends when the difference of the probability distribution parameters between two iterations meets the following condition:

$$
\max\left(\left| \Theta_k^{(t+1)} - \Theta_k^{(t)} \right| \right) < \varepsilon, \forall k \in \{1, 2, \cdots, M\}, \quad (4)
$$

where ε represents the threshold error.

After calculating the parameters of every single Gaussian distribution with the EM algorithm, the Gaussian mixture distribution model of the first departure time of the day can be obtained.

2) TRAVEL DESTINATION TYPE

This article considers Q types of travel destinations, i.e. $p_i \in \{D_1, D_2, \ldots, D_j, \ldots, D_Q\}$, wherein $p_i = D_j$ means the

destination of the i-th trip is D_j. The transition probability of the i-th trip $P[p_i|p_{i-1}, T_{s,i}]$ between different destinations is a conditional probability based on the departure time $T_{s,i}$. Therefore, this article divides a day into H periods and calculates the frequency of travel records in each period. Then, an $H \times Q \times Q$ transition probability matrix R can be created, where the element $r_{k,i,j}$ is the travel transition probability from D_i to D_j during the period of $[t_{k-1}, t_k]$.

TABLE 1. The most common travel destination types.

Proportion	Home /%	Work /%	Shopping /%	Entertainment /%	Pick-up /%	Dining /%	Sum /%
Weekday	32.34	17.90	16.05	8.67	7.73	7.36	90.05
Weekend	37.31	3.88	20.34	14.50	4.50	10.77	91.30

The most common travel destination types on weekdays and weekends are given in Table 1 sorted by frequency. It can be seen that the 6 types of travel destinations have a cumulative probability of 90%, and there is a clear difference between weekdays and weekends. Herein, it is assumed that the destination for each trip in the trip chains is one of the 6 types, i.e. $Q = 6$.

It is assumed that the starting and ending locations of the trip chain are both Home. However, a trip with Home as the destination does not necessarily mean Home is the end of the trip chain. Taking this into consideration, trips with Home as the destination are further divided into two categories: a) Home[a]: temporary parking at home; b) Home[b]: return home and end the current trip chain. Therefore, the transition probability matrix R can be expanded as $H \times Q \times (Q+1)$.

3) DRIVING TIME AND MILEAGE
The driving time $t_{v,i}$ follows a log-normal distribution when the departure type p_{i-1} and destination type p_i of the i-th trip are determined [17], i.e. $\ln(t_{v,i}) \sim N[\mu_v(p_{i-1}, p_i), \sigma_v^2(p_{i-1}, p_i)]$ which takes the uncertain factors into account, such as driving habits, traffic jam, and different distances to the same destinations.

The driving mileage d_i follows a normal distribution when the driving time $t_{v,i}$ is determined, i.e. $d_i \sim N[\mu_d(t_{v,i}), \sigma_v^2(t_{v,i})]$, and the power function characteristics are satisfied between $\mu_d(t_v)$ with t_v, and $\sigma_d(t_v)$ with t_v as shown in Figure 4. The driving time is divided into several equally spaced segments, and the power function form $y(t_v) = a \times t_v^b$ is used to fit the distribution parameters of the driving mileage in each segment [17].

4) PARKING DURATION
The length of parking depends on the type of travel destination, i.e. where it is parked. As shown in Figure 5, the parking durations at destinations of Home[a], Shopping, Entertainment and Pick-up follow log-normal distributions. The parking durations at destinations of Work and Dining follow Gaussian mixed distributions composed of 3 and 2 single Gaussian distributions. It should be noticed that for the i-th
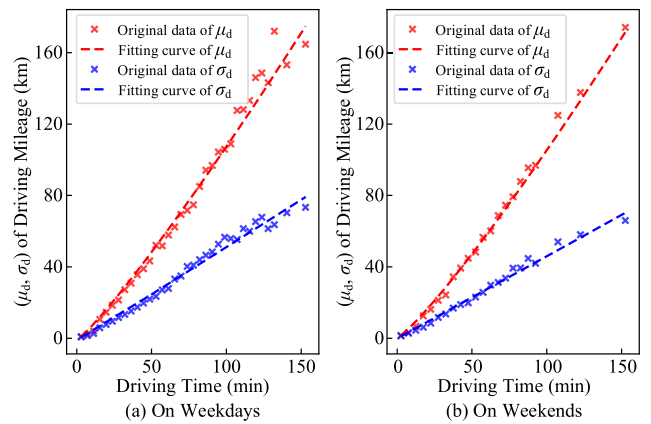

FIGURE 4. Power function relationship between driving mileage and driving time.
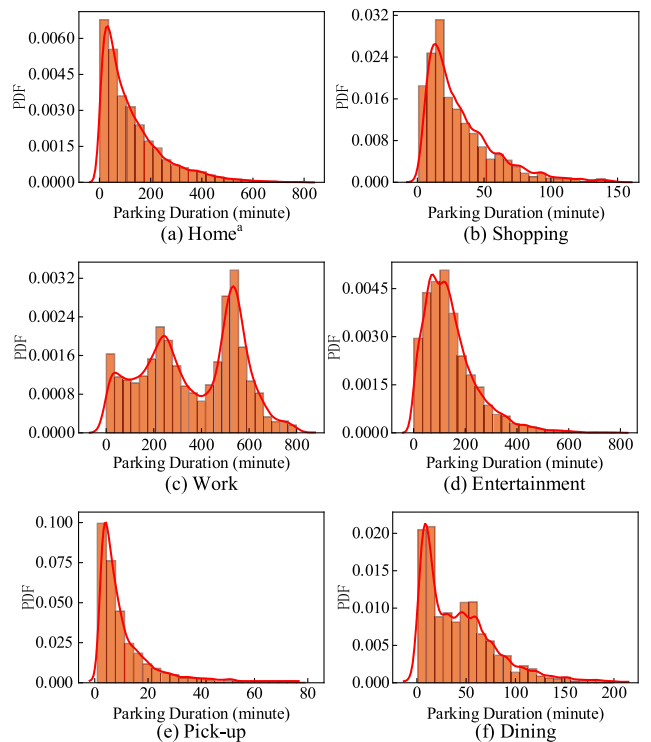

FIGURE 5. PDF histograms of parking durations at different destinations.

trip with Home[b] as the destination, the parking duration $t_{p,i}$ is determined by the first departure time of the next day.

5) THE DIFFERENCE BETWEEN WEEKDAYS AND WEEKENDS
Data shows that there is a clear difference between the travel preferences on weekends and weekdays. Therefore, each of the above-mentioned characteristic variables needs to be fitted separately.

Besides, since the daily trips in the NHTS 2017 dataset are evenly surveyed, the ratio between the number of daily trips that occur on weekdays and weekends can reflect the user's preference difference for starting a trip chain between weekdays and weekends. Therefore, we define the probability of starting a trip chain on weekdays as $P_1 = 1$. The probability

of starting a trip chain on weekends P_2 can be expressed as:

$$P_2 = \frac{N_{\text{wke}}/2}{N_{\text{wkd}}/5} P_1, \tag{5}$$

where N_{wke} and N_{wkd} are the numbers of travel records on weekends and weekdays.

III. EV SCHEDULING STRATEGY BASED ON THE FIVE-ZONE MAP

A. MODEL OF THE FIVE-ZONE MAP

In order to intuitively reflect the ability of EVs responding to AGC signals and participating in V2G under the premise of meeting the owner's travel needs, an EV scheduling strategy based on the five-zone map is proposed as a new solution. When the EV is plugged into the power grid, it will upload necessary information such as whether it will participate in V2G, the expected off-grid time and the expected off-grid SOC to the charging pile. EV's five-zone map is illustrated in Figure 6.
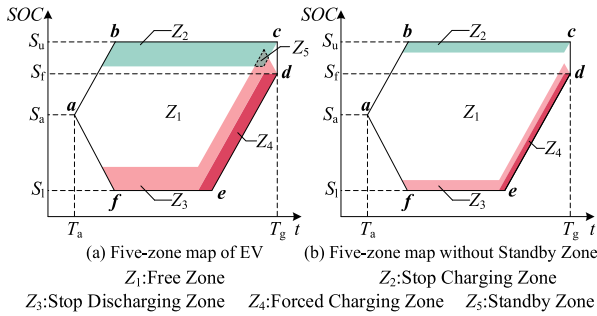

FIGURE 6. Five-zone map of EV.

In Figure 6(a), S_l and S_u are the minimum and maximum SOCs during V2G, T_a and T_g are the time when the EV is connected to and disconnected from the grid. S_a is the SOC when it is connected to the grid, and S_f is the lowest SOC meets the user's travel demand when it is disconnected from the grid. The closed area Z formed by the polyline **abcdef** represents the safe operating zone based on the SOC during the on-grid time, where the line segments **bc** and **fe** represent the upper and lower boundary of the SOC, and the line segment **ed** represents the forced-charging boundary, the line segment **dc** represents the SOC range when the EV is disconnected from the grid.

Assuming the slope of line segments **ab** and **ed** is k_c, and the slope of line segment **af** is k_d, which can be expressed as:

$$\begin{cases} k_{\text{c}} = \dfrac{\eta_{\text{c}} P_{\text{c}}}{C_{\text{b}}} \\ k_{\text{d}} = -\dfrac{P_{\text{d}}}{\eta_{\text{d}} C_{\text{b}}} \end{cases}, \tag{6}$$

where η_{c} and η_{d} are the charging efficiency and discharging efficiency, P_{c} and P_{d} are the charging power and discharging power measured at the grid side, C_{b} is the EV battery capacity.

Each point $x(t, S_t)$ in zone Z is a charging state of EV, wherein S_t is the SOC at time t. The locations of the 6 boundary points of zone Z are given in Table 2.

TABLE 2. Boundary points of zone Z.

Boundary point	Coordinates
a	$(T_{\text{a}}, S_{\text{a}})$
b	$[T_{\text{a}} + (S_{\text{u}} - S_{\text{a}})/k_{\text{c}}, S_{\text{u}}]$
c	$(T_{\text{g}}, S_{\text{u}})$
d	$(T_{\text{g}}, S_{\text{f}})$
e	$[T_{\text{g}} - (S_{\text{f}} - S_{\text{l}})/k_{\text{c}}, S_{\text{l}}]$
f	$[T_{\text{a}} + (S_{\text{l}} - S_{\text{a}})/k_{\text{d}}, S_{\text{l}}]$

The on-grid period of the EV is divided into several sub-control periods with intervals of T. The behavior of EV in each sub-control period can be charging, discharging and standby. According to different results caused by different behaviors of EV in each sub-control period, the zone Z can be divided into five sub-zones, i.e. free zone Z_1, stop charging zone Z_2, stop discharging zone Z_3, forced charging zone Z_4 and standby zone Z_5. The criteria for dividing each zone are described as follows:

1) STOP CHARGING ZONE Z_2

Charging in the stop charging zone will cause the SOC to be higher than the upper limit S_u. Therefore, the charging behavior should be stopped in this zone. The criterion that the charging state of the EV at time t in the stop charging zone $x(t, S_t) \in Z_2$ can be expressed as:

$$\begin{cases} S_u - k_c T \leq S_t \leq k_c(t - T_a) + S_a, \\ \qquad T_a + \dfrac{S_u - S_a}{k_c} - T \leq t \leq T_a + \dfrac{S_u - S_a}{k_c} \\ S_u - k_c T \leq S_t \leq S_u, \\ \qquad T_a + \dfrac{S_u - S_a}{k_c} < t \leq T_g - T \\ k_c(t - T_g) + S_u \leq S_t \leq S_u, \\ \qquad T_g - T < t \leq T_g \end{cases}, \tag{7}$$

2) STOP DISCHARGING ZONE Z_3

Discharging in the stop discharging zone will cause the SOC to be lower than the limit S_l or the SOC cannot meet the travel need when the EV is disconnected from the grid. Therefore, the discharging behavior should be stopped in this zone. The criterion that the charging state of the EV at time t in the stop discharging zone $x(t, S_t) \in Z_3$ can be expressed as:

$$\begin{cases} k_d(t - T_a) + S_a \leq S_t \leq S_l - k_d T, \\ \qquad T_a - T + \frac{S_l - S_a}{k_d} \leq t \leq T_a + \dfrac{S_l - S_a}{k_d} \\ S_l \leq S_t \leq S_l - k_d T, \\ \qquad T_a + \frac{S_l - S_a}{k_d} < t \leq T_g - \frac{S_f - S_l}{k_c} - T \\ k_c(t - T_g + T) + S_f \leq S_t \leq k_c(t - T_g + T) + S_f - k_d T, \\ \qquad T_g - \dfrac{S_f - S_l}{k_c} - T < t \leq T_g - T \\ S_f \leq S_t \leq k_d(t - T_g) + S_f, \\ \qquad T_g - T < t \leq T_g \end{cases}, \tag{8}$$

3) FORCED CHARGING ZONE Z_4

Discharging or standby in the forced charging zone will cause the SOC to reach the forced-charging boundary ed. The criterion that the charging state of the EV at time t in the forced charging zone $x(t, S_t) \in Z_4$ can be expressed as:

$$\begin{cases} S_l \le S_t \le k_c \left(t - T_g + T\right) + S_f, \\ \qquad T_g - \dfrac{S_f - S_l}{k_c} - T \le t \le T_g - \dfrac{S_f - S_l}{k_c} \\ k_c \left(t - T_g\right) + S_f \le S_t \le k_c \left(t - T_g + T\right) + S_f, \\ \qquad T_g - \dfrac{S_f - S_l}{k_c} < t \le T_g - T \\ k_c \left(t - T_g\right) + S_f \le S_t \le S_f, \\ \qquad T_g - T < t \le T_g \end{cases}, \tag{9}$$

4) STANDBY ZONE Z_5

The existence of the standby zone depends on the value of the sub-control period T. If T meets the condition in (10), the stop charging zone Z_2 and the stop discharging zone Z_3 will form a closed intersection zone, which is the standby zone. Charging or discharging in the standby zone will cause the SOC to reach the limit S_u or the forced-charging boundary ed. If T does not meet the condition in (10), the standby zone will not exist. The five-zone map without Z_5 is shown in Figure 6(b).

$$T > \frac{S_u - S_f}{k_c - k_d}, \tag{10}$$

If the standby zone Z_5 exists, the criterion that the charging state of the EV at time t in the standby zone $x(t, S_t) \in Z_5$ can be expressed as:

$$\begin{cases} S_u - k_c T \le S_t \le k_c \left(t - T_g + T\right) + S_f - k_d T, \\ \qquad \dfrac{S_u - S_f - (k_c - k_d)\, T}{k_c} + \left(T_g - T\right) \le t \le T_g - T \\ k_c \left(t - T_g\right) + S_u \le S_t \le k_d \left(t - T_g\right) + S_f, \\ \qquad T_g - T < t \le T_g + \dfrac{S_u - S_f}{k_d - k_c} \end{cases}, \tag{11}$$

5) FREE ZONE Z_1

The other area in Z is regarded as the free zone Z_1, where EVs can choose to charge, discharge or standby. The free zone Z_1 can be expressed as:

$$Z_1 = Z \backslash \left(Z_2 \cup Z_3 \cup Z_4 \cup Z_5\right), \tag{12}$$

B. BEHAVIORAL DECISION-MAKING IN FIVE-ZONE MAP

1) FREE ZONE Z_1

The decision-making strategy of charge and discharge behavior in the free zone is shown in Figure 7(a). Point A represents the charging state of the EV at the initial moment of the period of $[nT, (n + 1)T]$. Segments AB, AC, and AD represent the SOC updating trace with the EV's state being charging, discharging, and standby. None of the three behaviors will reach the boundary of Z. Therefore, any behavior can be selected in the free zone.

2) STOP CHARGING ZONE Z_2

The decision-making strategy of charge and discharge behavior in the stop charging zone is shown in Figure 7(b). The upper boundary of zone Z can be reached with the battery being charged during the period of $[nT, (n+1)T]$. Therefore, the battery should be charged first and then standby during this period, as shown by line ABD. Discharge or standby can also be selected in the stop charging zone.

3) STOP DISCHARGING ZONE Z_3

The decision-making strategy of charge and discharge behavior in the stop discharging zone is shown in Figure 7(c). The lower boundary of zone Z can be reached with the battery being discharged during the period of $[nT, (n + 1)T]$. Therefore, the battery should be discharged first and then standby during this period, as shown by line ACD. Charge or standby can also be selected in the stop discharging zone.

4) FORCED CHARGING ZONE Z_4

The decision-making strategy of charge and discharge behavior in the forced charging zone is shown in Figure 7(d). The forced-charge boundary ed can be reached both with the battery being discharged or standby during the period $[nT, (n + 1)T]$. Therefore, the battery should be charged during this period, as shown by line AB.

5) STANDBY ZONE Z_5

In the standby zone, EV should remain standby to ensure the SOC will not reach the boundary of the zone Z.

IV. CHARGE AND DISCHARGE CAPACITY OF EV CLUSTER

A. ANALYSIS OF THE CHARGE AND DISCHARGE BEHAVIOR

The SOC at the arrival time of the i-th trip can be expressed as:

$$S_{T_{a,i}} = S_{T_{s,i}} - \frac{\upsilon d_i}{100 C_b}, \tag{13}$$

where $S_{T a,i}$ and $S_{T s,i}$ are the SOC at the arrival time and departure time of the i-th trip, $S_{T a,i}$ is considered to be higher than 15% to ensure the safety of driving, d_i is the diving mileage of the i-th trip (km), υ is the power consumption per 100 kilometers (kWh/100km) and C_b is the battery capacity (kWh).

In this article, two charging modes are considered, i.e. slow charging with AC power of P_c and fast charging with DC power of P'_c.

For EVs do not participate in V2G, their charging behavior depends on the SOC level $S_{T a,i}$ and the usual initial charging SOC S_s. Their discharge capacity is regarded as zero.

For EVs participate in V2G, when arriving at the destination, information of T_a, T_g, S_l, S_u, S_a, and S_f are uploaded to the charging pile. Then, the five-zone map can be obtained based on (6)-(12). The charging or discharging behavior in each sub-control interval can be determined according to the five-zone map scheduling strategy during the parking. It is
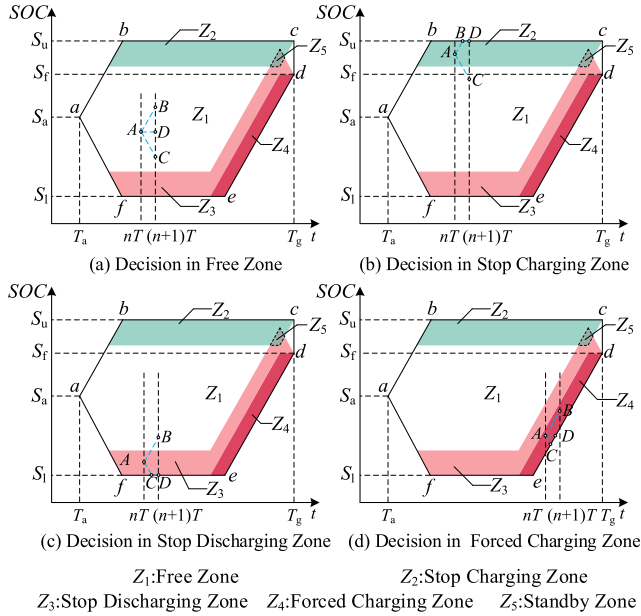
FIGURE 7. Behavioral decision-making in the five-zone map.

Z_1:Free Zone Z_2:Stop Charging Zone
Z_3:Stop Discharging Zone Z_4:Forced Charging Zone Z_5:Standby Zone

(a) Decision in Free Zone
(b) Decision in Stop Charging Zone
(c) Decision in Stop Discharging Zone
(d) Decision in Forced Charging Zone

assumed that the AGC signals of the power grid for the EV cluster are known, and the authority to decide the charging or discharging behavior is granted to the charging pile.

The analysis of the charging and discharging behavior of an individual EV is shown in Figure 8. When the parking is over, the charging and discharging power profile of the EV can be calculated by merging the behaviors during the parking.

B. CALCULATION PROCESS OF THE CHARGE AND DISCHARGE CAPACITY

According to the above methods, the simulation steps of the trip chains and the calculation steps of the charge and discharge capacity can be described as follows:

1) Fit characteristic variables of the trip chain, including the first departure time of the day, the trip transition probability, the driving time and mileage, and the parking duration.

2) Start to model trip chains. Specify the max simulation time as T_{max}, the number of EVs as N, and the current EV index as $n = 1$.

3) Draw a sample of the first departure time of the day $T_{s,1}$, and set the current trip index as $i = 1$.

4) Draw samples of the travel destination p_i, driving time $t_{v,i}$, and driving mileage d_i of the i-th trip, calculate the arrival time as $T_{a,i} = T_{s,i} + t_{v,i}$.

5) If the destination p_i is Home[b], then end the current trip chain and start a new trip chain for the next day; otherwise, go to 6).

6) Draw a sample of the parking duration $t_{p,i}$, calculate the end time of the i-th trip as $T_{g,i} = T_{a,i} + t_{p,i}$.

7) If the current time $T_{g,i}$ exceeds the max simulation time T_{max}, go to 9); otherwise, go to 8).

8) Calculate the departure time of the $(i + 1)$-th trip as $T_{s,i+1} = T_{g,i}$, and let $i = i+1$, then go to 4).

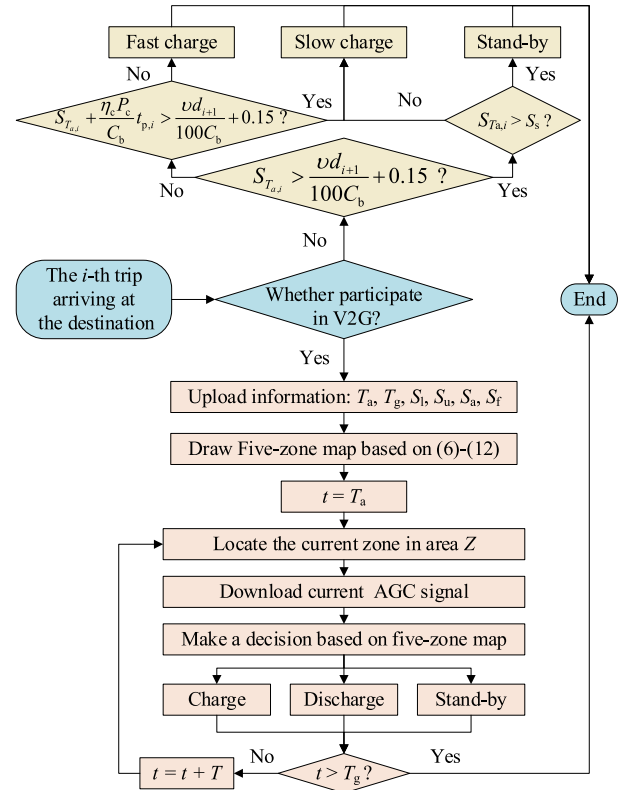**FIGURE 8.** Analysis of the charging and discharging behavior of an individual EV.

9) If the current EV index n exceeds N, go to 10); otherwise, let $n = n+1$ and go to 3).

10) Start to calculate charge and discharge capacity. Let $n = 1$.

11) Specify I as the number of trips of the n-th EV in the cluster.

12) Initialize the SOC at the departure time of the first trip to 1, and let the trip index $i = 1$.

13) Calculate the SOC at the arrival time of the i-th trip based on (13).

14) Determine the charging and discharging behaviors, and calculate the charging and discharging power profile during the parking according to Figure 8.

15) If the current trip index i exceeds I, go to 16); otherwise let $i = i+1$ and go to 13).

16) If the current EV index n exceeds N, then calculate the charging and discharging power profile of the EV cluster; otherwise, let $n = n+1$ and go to 11).

The flowchart of the charge and discharge capacity calculation is depicted in Figure 9.

V. CASE STUDY

The charge and discharge capacity of EV clusters is calculated based on the NHTS dataset released by the Federal Highway Administration in 2017.

A. PARAMETERS OF THE EV CLUSTER

According to a report from the International Council on Clean Transportation (ICCT) on the American EV market [33], the
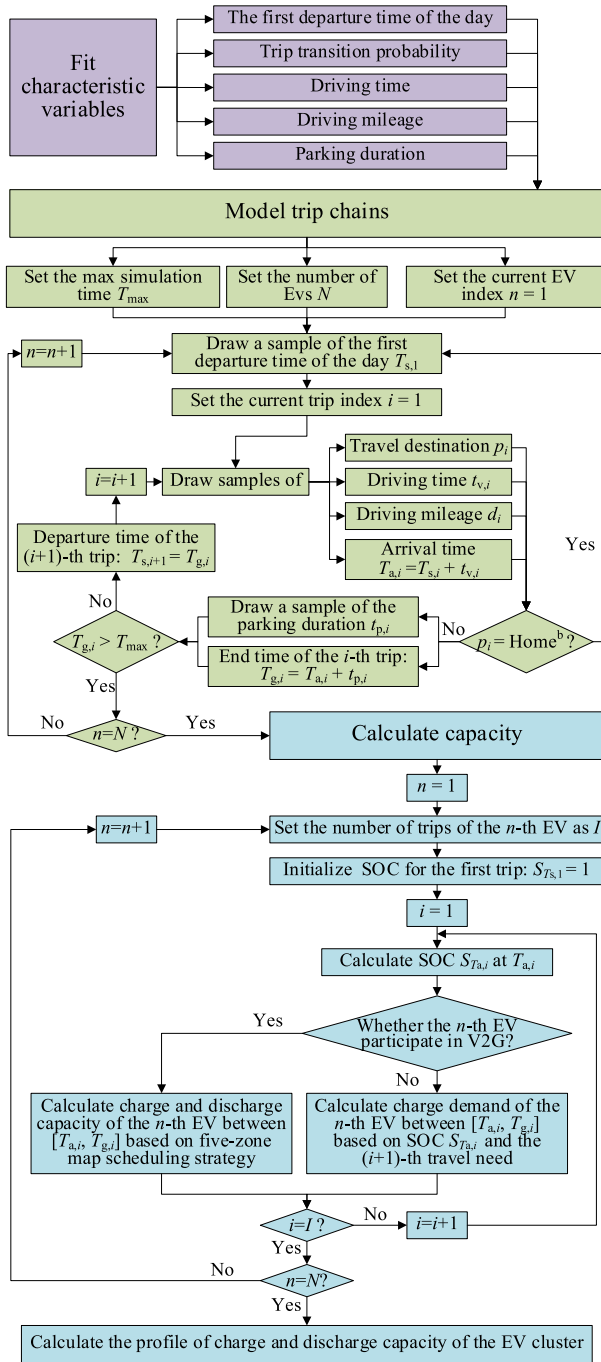
FIGURE 9. Flowchart of the charge and discharge capacity calculation.

top five EV models with the highest market share are used for modeling EV clusters. Their battery parameters are listed in Table 3. The power of slow charge and fast charge are set to 5kW and 50kW respectively. The size of the EV cluster is set to 5000, and the proportion of various types of vehicles in the cluster is determined according to the market share.

According to the EV Project Nissan Leaf Vehicle Summary Report jointly released by Nissan and the Office of Energy Efficiency & Renewable Energy [34], the usual initial charging SOC S_s of EV owners normally follows a normal distribution, i.e. $S_s \sim N(0.48, 0.152^2)$.

TABLE 3. Battery parameters of top 5 types of EVs.

EV models	Proportion of quantity	Battery capacity (kWh)	Power efficiency (kWh/100km)
Tesla Model 3	63.0%	75	16
Tesla Model X	11.2%	100	24
Tesla Model S	11.0%	100	15.4
Chevrolet Bolt	8.1%	66	17.2
Nissan Leaf	6.7%	30	21.2

The timeslot for observing SOC is set to 1 minute, and the maximum simulation time is set to 3 weeks.

B. FITTING THE PROBABILITY DISTRIBUTION PARAMETERS

1) DATA CLEANING

Trips of which the driving time and mileage are valid values (i.e. non-zero or non-null value) with private cars are selected from the dataset, including a total of 601,071 trips on weekdays and 183,777 trips on weekends. Hence, the probability of a weekend trip is 0.764 according to (5).

2) TRAVEL DESTINATION TYPES

As mentioned before in Section II.B, it is assumed that the destination for each trip is one of the 6 most common types, i.e. Home, Work, Shopping, Entertainment, Pick-up, and Dining. Home is further divided into Home[a] and Home[b].

Travel transition probability among different destinations varies over time. Dividing a day into 24 periods, the trip transition probabilities between destinations in each period of weekdays and weekends are calculated. The comparison of travel transition probabilities in 08:00-09:00 and 14:00-15:00 on weekdays and weekends is shown in Figure 10. The peak value of the red curve in Figure 10(a) is 0.585, which means a trip taking "Home" as the departure has a probability of 58.5% of taking "Work" as the destination during the period of 08:00-09:00. It can be seen that the choice of the travel destination is closely related to the type and time of the departure.

3) THE FIRST DEPARTURE TIME OF THE DAY

The EM algorithm is used to fit the first departure time of the day which follows a one-dimensional Gaussian mixture distribution composed of 3 single Gaussian distributions, the distribution parameters in hours are shown in Table 4. The PDF histograms based on these parameters are shown in Figure 11.

TABLE 4. Distribution parameters of the first departure time of the day.

Parameters	θ_1			θ_2			θ_3		
	ω_1	μ_1	σ_1	ω_2	μ_2	σ_2	ω_3	μ_3	σ_3
Weekdays	0.36	7.42	0.91	0.43	8.63	1.99	0.21	13.07	3.10
Weekends	0.79	9.51	1.89	0.12	13.99	1.36	0.10	17.36	1.84

4) DURATION OF PARKING AT DIFFERENT DESTINATIONS

As mentioned in Section II.B, models of log-normal distributions and Gaussian mixed distributions composed of 3 and
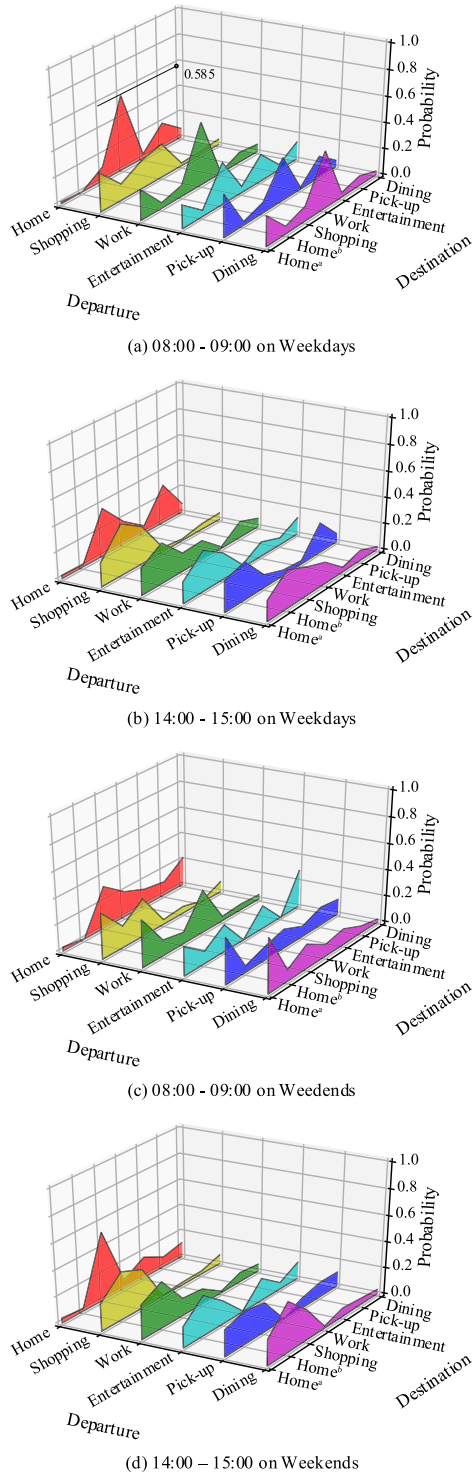
(a) 08:00 - 09:00 on Weekdays

(b) 14:00 - 15:00 on Weekdays

(c) 08:00 - 09:00 on Weedends

(d) 14:00 − 15:00 on Weekends

FIGURE 10. Travel transition probabilities in typical periods.

2 single Gaussian distributions are used to fit the parking duration under different types of destinations. The parameters of the probability distributions are shown in Table 5.

5) DRIVING TIME AND MILEAGE

The driving time t_v between different departure and destination types follows the log-normal distribution, the parameters
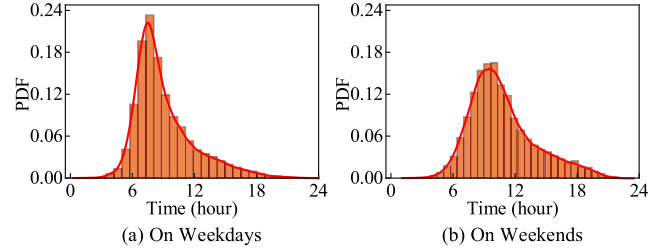

FIGURE 11. PDF histograms of the fitted daily first departure time.

TABLE 5. Distribution parameters of parking duration.

Destinations	Distribution Types		Weekdays	Weekends
Home[a] (minute)	Log-normal	μ	4.34	4.48
		σ	1.15	1.13
Shopping (minute)	Log-normal	μ	3.11	3.20
		σ	0.90	0.92
Work (hour)	Gaussian mixed distributions composed of 3 single distributions	ω_1	0.12	0.13
		μ_1	0.72	0.54
		σ_1	0.51	0.41
		ω_2	0.38	0.30
		μ_2	3.75	3.13
		σ_2	1.25	1.40
		ω_3	0.50	0.57
		μ_3	8.91	8.02
		σ_3	1.54	2.37
Entertainment (minute)	Log-normal	μ	4.65	4.71
		σ	0.96	0.96
Pick-up (minute)	Log-normal	μ	1.81	1.90
		σ	1.23	1.27
Dining (hour)	Gaussian mixed distributions composed of 2 single distributions	ω_1	0.51	0.51
		μ_1	0.31	0.47
		σ_1	0.23	0.34
		ω_2	0.49	0.49
		μ_2	1.12	1.33
		σ_2	0.73	0.88

TABLE 6. Power function parameters of driving mileage.

Trip days	μ_d			σ_d		
	a	b	M_{AE}	a	b	M_{AE}
Weekdays	0.2622	1.2602	1.2091	0.1500	1.2476	0.3615
Weekends	0.1677	1.3956	0.7378	0.2019	1.1571	0.3777

of which are listed in Appendix B. Dividing the driving time of all trips into several levels at a five-minute interval and calculating the average mileage of each level, the power function is used to fit the relationship between mileage and driving time, and the average absolute error (MAE) is calculated. The fitted parameters are shown in Table 6.

Therefore, the driving mileage on weekdays and weekends follow the conditional normal distribution as below:

$$N[0.2622 \times t_v^{1.2602}, (0.1500 \times t_v^{1.2476})^2],$$
$$N[0.1667 \times t_v^{1.3956}, (0.2019 \times t_v^{1.1571})^2].$$

C. SIMULATION OF THE TRIP CHAIN

The simulation of the EV cluster trip chain follows the steps shown in Figure 9. The mileage for each trip is selected as the verification object. The probability density function and
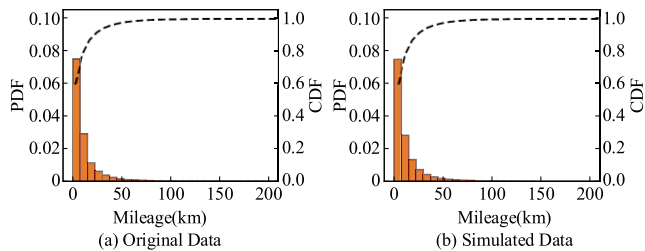
FIGURE 12. Comparison of trip mileage in original and simulated data.
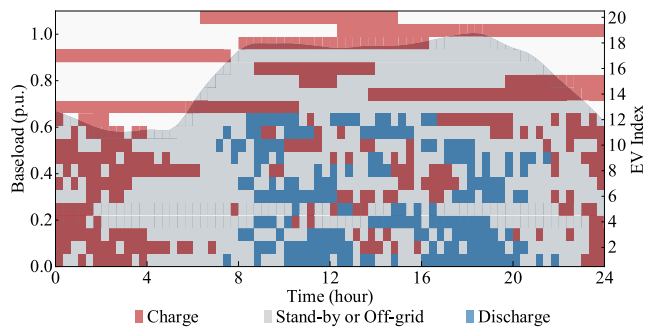

FIGURE 13. Charge and discharge behaviors of 20 selected EVs.

cumulative distribution function (CDF) of the mileage in the original and the simulated data are shown in Figure 12, which shows that the simulated trip chains conform to the actual driving law.

D. CALCULATION OF THE CHARGE AND DISCHARGE CAPACITY

It is assumed that owners charge or discharge only in residential areas, working areas, shopping areas, and entertainment areas, and do not charge or discharge during pick-up and meals. To reduce the impact of the simulation initialization and compare the results on weekdays and weekends, the charge and discharge capacity of the EV cluster on the second Tuesday and the third Saturday are analyzed.

To illustrate the implementation of the proposed V2G scheduling strategy, 20 EVs are randomly selected from the EV cluster, in which No.1-12 will participate in V2G, and No.13-20 will not. The charging and discharging behaviors of the selected EVs within 24 hours of the second Tuesday are drawn in a heat map together with the baseload of the grid, as shown in Figure 13.

It can be seen that during the on-peak period of the baseload, most of EVs No.1-12 discharge to feed energy back to the grid, and a few of them charge to ensure the users' travel needs. During the off-peak period of the baseload, EVs No.1-12 charge to fill the valley of load curve and prepare for next day's trips. The charging decisions of EVs No.13-20 depend on the users' travel needs, and no discharging decision is made.

The proportion of EVs participating in V2G in the cluster is usually affected by objective factors such as the driving demand, electricity price, and battery anti-aging technology. Studies in [35]–[37] have shown that optimistic discharge

incentive policies can increase this proportion. In this article, the proportion of EVs participating in V2G in the cluster is defined as K_p, which is regarded as an adjustable preset parameter to analyze the charge-discharge capability under different objective conditions. K_p can be expressed as:

$$K_p = \frac{N_p}{N}, \qquad (14)$$

where N_p is the number of EVs participating in V2G in the cluster; N is the size of the EV cluster, i.e. the total number of EVs in the cluster.

The charge and discharge capacity on weekdays and weekends in each area when $K_p = 0.6$ are shown in Figure 14, and the proportion of energy charged and discharged in each area are listed in Table 7.
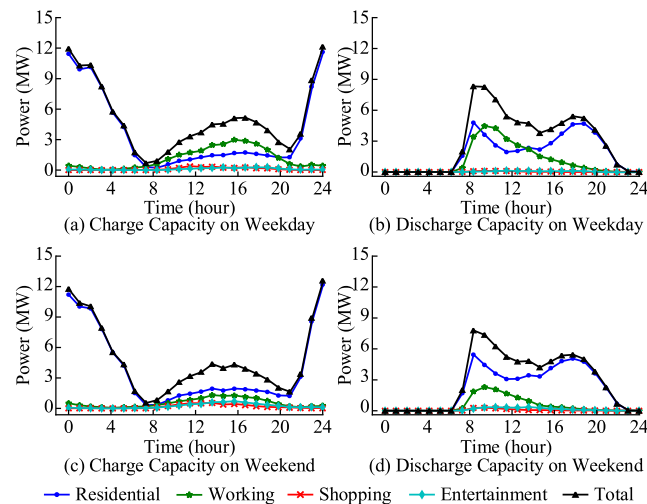

FIGURE 14. Charge and discharge capacity of EV cluster.

TABLE 7. Proportion of energy charged and discharged in each area.

Areas	Weekday (%)		Weekend (%)	
	Charge	Discharge	Charge	Discharge
Residential	70.8%	60.5%	78.5%	76.9%
Working	24.2%	36.8%	12.3%	17.1%
Shopping	2.4%	1.0%	3.8%	1.8%
Entertainment	2.6%	1.7%	5.4%	4.2%

In line with the AGC signals from the power grid, the charge power of the cluster is concentrated on the off-peak period of the baseload, i.e. 22:00 to 06:00 the next day, and the discharge power of the cluster is concentrated on the on-peak period of the baseload, i.e. 08:00-20:00. The short parking duration and the small number of EVs lead to low charging and discharging power in shopping and entertainment areas.

During the off-peak period of the baseload, the power grid releases AGC signals of charging, EVs participating in V2G are charged during this period to meet their daytime travel needs. Since most EVs are at home during this period, the energy charged in the residential area accounts for a proportion of 95.1% in all areas.

During the on-peak period of the baseload, the power grid releases AGC signals of discharging. The discharge capacity in the working area on weekends is lower than on weekdays,

and the energy-discharged in the working area on weekdays increases by 19.7% compared to weekends. The discharge capacity in the working area in the morning is higher than that in the afternoon. This is because a large number of EVs arrive at the working area in the morning and feed the remaining power back to the grid. They charge in the afternoon to meet the travel needs after work.

Besides, some owners set off late in the morning and some owners end their trips in the early evening, which causes two peaks in the discharge capacity profile in the residential area.

E. CHARGE AND DISCHARGE CAPACITY IN DIFFERENT SITUATIONS

1) CHARGE AND DISCHARGE CAPACITY WITH DIFFERENT K_P

When $K_p = 0$, it is considered that the discharge capacity of the EV cluster in response to the AGC signals is zero. Charge demand comes from uncoordinated charging of EVs. The charge demand on weekdays and weekends in each area is shown in Figure 15, and the proportion of energy charged in each area are listed in Table 8.
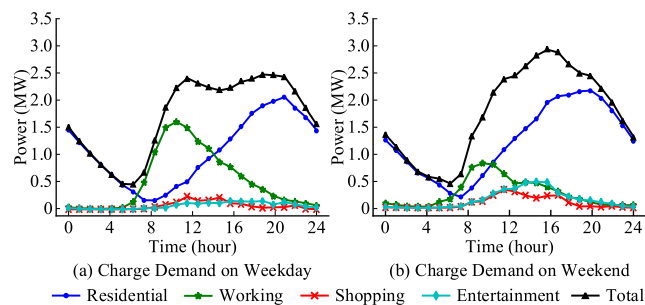

FIGURE 15. Charge and discharge capacity of EV cluster when $K_p = 0$.

TABLE 8. Proportion of energy charged in each area.

Areas	Weekdays (%)	Weekends (%)
Residential	59.8%	69.8%
Working	32.7%	16.0%
Shopping	3.6%	5.5%
Entertainment	3.9%	8.7%

It can be seen that the peak charging load in the residential area appears around 20:00 and is the highest among these areas. The peak charging load in the working area appears around 10:00. The energy-charged on weekends in the working area decreased by 16.7% than weekdays, which results in a 10.0% increase in energy-charged in the residential area. The charging demand in shopping and entertainment areas is low, and the peak load appears in the afternoon. The proportion of energy-charged in these two areas has increased from 7.5% on weekdays to 14.2% on weekends. However, it is still lower than in other areas.

There is a significant peak-to-valley difference in the daily charge demand profile. The charge demand is high in the daytime and evening and low in the early morning. The peak of the total charge demand on weekends is about 1.5 to 2 hours later than on weekdays. The energy-charged in working area accounts for 32.7% on weekdays, a decrease to
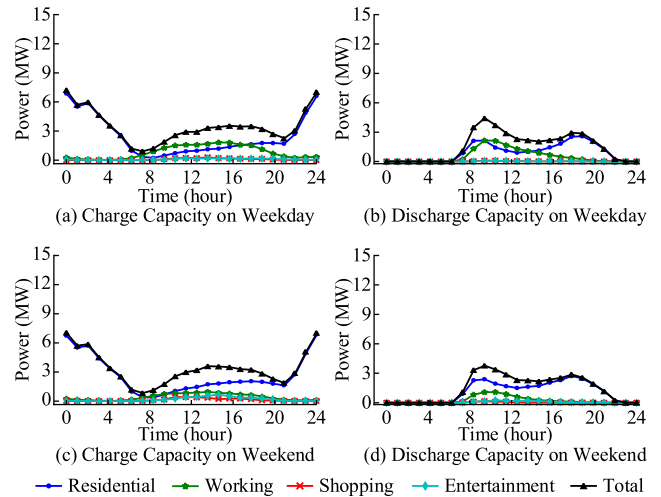

FIGURE 16. Charge and discharge capacity of EV cluster when $K_p = 0.3$.

16.0% on the weekends leads to the daily load curve changing from a double-peak to a single-peak, and the peak-to-valley difference increasing by 10.9%.

When $K_p = 0.6$, the charge and discharge capacity of EV cluster on weekdays and weekends in each area is shown in Figure 14. It should be noticed that, because the power grid released AGC signals of charging during the off-peak period of the baseload, the energy-charged in the residential area has increased by 166.5% compared to the case when $K_p = 0$, which helps to reduce the wind power curtailment at night.

When $K_p = 0.3$, the charge and discharge capacity of EV cluster on weekdays and weekends in each area is shown in Figure 16. The energy charged and discharged on weekdays have decreased by 29.5% and 48.2% compare to the case when $K_p = 0.6$.

2) CHARGE AND DISCHARGE CAPACITY WITH DIFFERENT CLUSTER SIZE N

When $K_p = 0.6$, the charge and discharge capacity and energy on weekdays of the cluster with different sizes N are shown in Figure 17. With the increase of cluster size, the charge capacity during the off-peak period of the baseload and the discharge capacity during the on-peak period have been greatly improved, which has significantly increased the dispatch capacity of the power grid. There is a strong linear correlation between the energy charged and discharged with the size N, which can be fitted as a linear function $y = \alpha x + \beta$ whose parameters and root mean square error R_{MSE} are given in Table 9.

TABLE 9. Linear function parameters of energy charged and discharged.

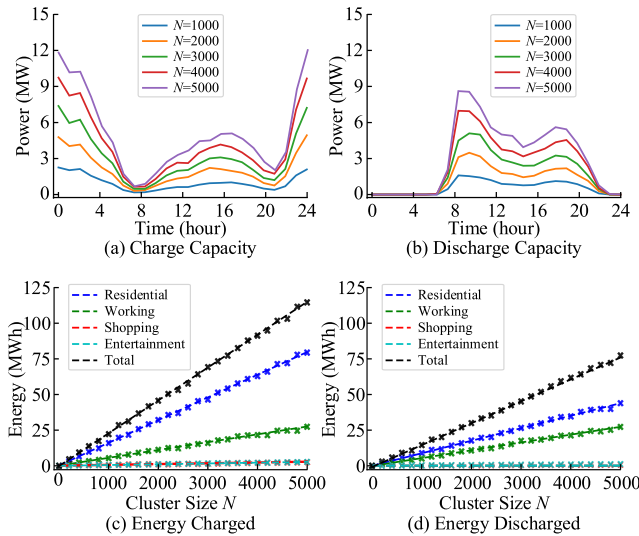| Areas	Energy charged			Energy discharged		
	α	β	R_{MSE}	α	β	R_{MSE}
Residential	0.0158	0.1281	0.6425	0.0087	0.0053	0.5330
Working	0.0054	0.0533	0.3319	0.0054	-0.1462	0.3305
Shopping	0.0005	0.0435	0.0612	0.0001	-0.0150	0.0245
Entertainment	0.0005	-0.0188	0.0575	0.0002	0.0412	0.0467
Total	0.0229	-0.3054	0.6672	0.0152	-0.9215	0.5850

FIGURE 17. Capacity and energy of EV cluster of different sizes.

F. COMPARISON WITH OTHER METHODS

1) CHARGE DEMAND

An EV charge demand model is proposed in [38], which assumes that the start charging time of EVs follows a normal distribution $N(17.5, 3.4^2)$, and the daily mileage follows a log-normal distribution $log\text{-}N(3.4, 0.5^2)$. Another EV charge demand model is proposed in [39], which assumes that 30% of the EVs in the cluster will charge in the working area where the start charging time follows a normal distribution $N(9, 0.5^2)$, and 70% will charge in the residential area where the start charging time follows a normal distribution $N(19, 1.5^2)$. Besides, the initial charging SOC follows the normal distribution $N(0.6, 0.1^2)$. Neither model can calculate the discharge capacity of EV clusters.

A comparison of the charge demand results between the proposed model and the other two models has been carried out. Assuming that the size of the EV cluster is 5000. The charge demand of different models on weekdays are shown in Figure 18, and the energy charged are given in Table 10.

TABLE 10. Energy-charged of different models.

Models	Energy charged / MWh
In this paper	40.7
In [38]	39.1
In [39]	50.5

It can be seen that the energy-charged in [38] are close to the results in this article while the peak charging load appears in the early evening. This is because this model does not consider the charge demand in the working area.

Compared with the model in this article, the charge demand curve of the model in [38] has two peaks with higher peak values and higher energy-charged. This is because the model assumes that the initial charging SOC is concentrated around 0.6, but ignores the impact of the driving mileage on the charge demand. As the driving range of EVs increases, owners will allow EVs to start charging at lower SOC levels.
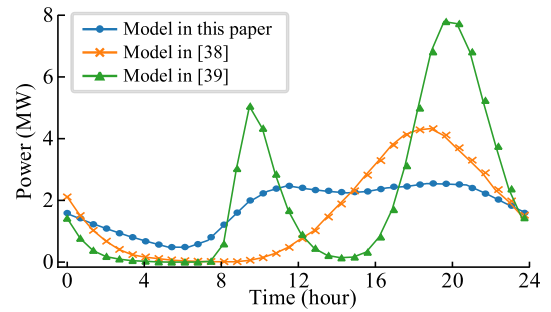

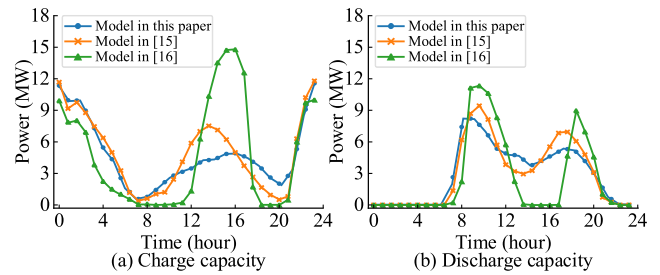**FIGURE 18. Comparison of charge demands of different models.**

FIGURE 19. Comparison of charge and discharge capacity of different models.

Therefore, the rationality of the assumption in [39] needs to be further verified.

2) CHARGE AND DISCHARGE CAPACITY

A trip chain model is proposed in [15], which assumes that users do not travel more than 3 times in one day. The optional trip chains of this model include *Home-Work-Home*, *Home-Other-Home*, *Home-Work-Shopping-Home*, *Home-Other-Work-Home*, and length of other chains does not exceed 3. Another trip chain model is proposed in [16], which considers only two types of trip chains, i.e. *Home-Work-Home*, and *Home-Work-Shopping/Dining-Home*. The model assumes that the arrival time at the working area follows a uniform distribution $U(8, 9)$, and the departure time from the working area follows a uniform distribution $U(17, 18.5)$, and all EVs will return home before 22:30.

A comparison of charge-discharge capacity results between the proposed model and the other two models has been carried out. Assuming that the size of the EV cluster is 5000 and $K_p = 0.6$, the charge-discharge capacities of different models on weekdays are shown in Figure 19, and the energy charged and discharged are given in Table 11.

TABLE 11. Energy charged and discharged of different models.

Models	Energy charged / MWh	Energy Discharged / MWh
In this paper	114.0	73.2
In [15]	112.7	73.6
In [16]	110.6	63.4

It can be seen that the energy charged and discharged in [15] are close to the results in this article. However, by specifying the type of trip chains and limiting the number of daily trips, the model makes the distribution of users' departure and arrival times more concentrated. Therefore,

a peak appears in the daytime charging power curve, which is 37% higher than that in this article.

The model in [16] puts forward stricter restrictions on travel time distribution and the number of daily trips, which leads to an increase of 91% in the daytime charging power peak compared to [15]. The discharged-energy in its model is 13.4% lower than that in this article. This is because the model assumes that all EVs will leave the working area before 18:30. Therefore, the EVs which has been discharged are charged during 13:00-17:00 to meet travel needs, which results in charge capacity rises while discharge capacity falls. On the contrary, the model proposed in this article believes that not all users will leave the working area around 18:00, which meets the actual travel laws.

G. PARALLEL IMPLEMENTATION OF THE METHOD

The existing models need to fit travel characteristics from massive data and simulate the travel and charge-discharge behavior of large-scale EV clusters, which may cause huge calculation burdens. In recent years, the development direction of utilizing CPU computing power has shifted from increasing single-core frequency to balancing multi-core performance [40]–[42]. At the same time, cloud service providers such as Amazon Web Services, Microsoft Azure and Huawei Cloud can provide Elastic Cloud Server (ECS) to meet the need of differentiated computing [43]–[45]. Therefore, the proposed model is processed in parallel to increase the calculation speed. The computing platform is the ECS instance c6.4×large.4 provided by Huawei Cloud, which has 16 CPU cores based on Intel Cascade Lake clocked at 3.0 GHz, as well as 64 GB of memory and 40 GB of hard disk space. The operating system is CentOS 7.6.1810 (64-bit). A multi-process parallel computing environment is established based on Python 3.7. When the EV cluster size is 5000, the running time of each module in single-process serial mode is given in Table 12.

TABLE 12. Running time of each module in serial mode.

Modules	Functions	Running time (s)
M_1	Data cleaning	11.2
M_2	Fit characteristic variables	41.1
M_3	Trip chain simulation	187.4
M_4	Charge-discharge capacity	243.9
M_5	Visualization of results	16.7

It can be seen that the calculation of M_3 and M_4 modules takes longer time. Because the behaviors of EVs in the cluster are independent of each other, the simulation of travel and charge-discharge behaviors can be parallelized. Parallelizing the calculations of M_3 and M_4 wherein the C processes can run simultaneously and evenly distribute the computing tasks for each process. The calculation process of each module is shown in Figure 20.

The parallel acceleration ratio is defined as R_C to reflect the effect of multi-process on the calculation acceleration:

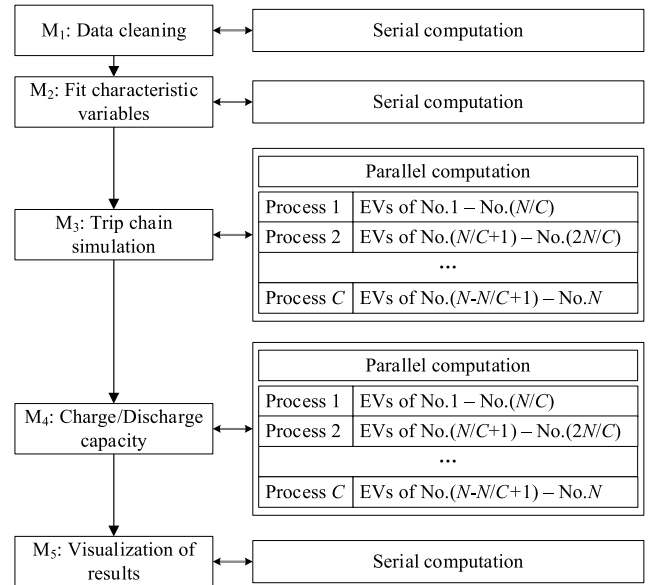$$R_C = \frac{T_1}{T_C}, \tag{15}$$

FIGURE 20. Calculation process of each module.

where T_1 is the total running time when only one process is allowed to create under certain cluster size N. T_C is the total running time when C processes are allowed to create simultaneously under the same cluster size N.
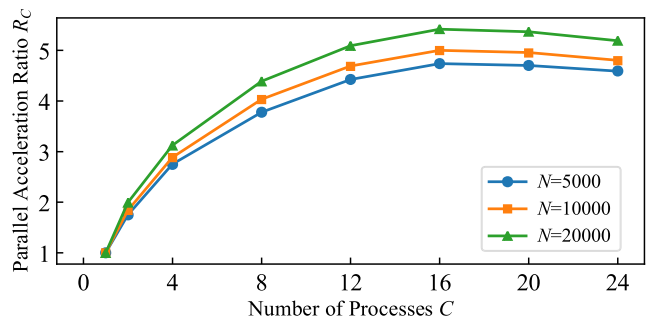

FIGURE 21. Parallel acceleration ratio under multiple processes.

Figure 21 shows the parallel acceleration ratio R_C under different numbers of processes C. It can be seen that:

1) R_C increases with the increase of the number of processes C. The acceleration effect is positively correlated with the cluster size, which proves the excellent parallel computing performance of the model.

2) When C is less than 16, i.e. the number of processes is less than the number of CPU cores, the growth rate of R_C decreases with the increase of C. This is because the proportion of the running time of the serial modules M_1, M_2, and M_5 increases with the increase of C.

3) When C is greater than 16, R_C decreases slowly. This is because the increased resources consumed by process management results in a decrease of the computing efficiency.

The results have proved the excellent parallel computing performance of the model. The number of processes should be set as close as possible to the number of CPU cores to achieve a higher computing efficiency.

VI. CONCLUSION

This article proposes a novel calculation model of charge and discharge capacity of EV clusters based on the trip chain. Based on the NHTS 2017 dataset, the characteristic variables of the trip chain are firstly fitted using probability distribution models. The trip chains of the EV cluster on a time scale of several weeks are simulated. In particular, a scheduling strategy based on the five-zone map is designed to calculate the charge and discharge capacities.

The following conclusions are unveiled by the studies:

1) The scheme based on the proposed five-zone map can guide the EV cluster to operate as an energy storage system by charging during off-peak periods and discharging or standing-by during on-peak periods, which increases with the growing of V2G participation rate K_p.

2) The charge capacity in the residential and working area accounts for a total proportion of around 93%. The discharge capacity of the working area in the morning is higher than that in the afternoon. There are two peaks in the daily discharge capacity curve of the residential area. The results have verified the effectiveness of the trip chain model in simulating the commuting characteristics of the residents.

3) It shows that there is a nonlinear correlation between the charge and discharge capacity with the cluster size, while there is a strong linear correlation between the energy charged and discharged with the cluster size.

4) The parallel acceleration ratio R_C under different number of processes C proves that the proposed model has excellent parallel computing performance.

The case study verifies the effectiveness of the model proposed. This work is suitable for evaluating the responsiveness of EV clusters to AGC signals, as well as the potential for providing frequency regulation. It would be high-efficient to apply the presented trip chain model to simulate the travel behavior of large-scale EV clusters on a long-term scale.

APPENDIX A
PROOF OF PARAMETER-ESTIMATION OF GAUSSIAN MIXTURE DISTRIBUTION BASED ON THE EM ALGORITHM

This is to demonstrate the parameter estimation of one-dimensional Gaussian mixture distribution composed of a finite number of M single Gaussian distributions.

Supposing the observation value of a one-dimensional Gaussian mixture distribution array composed of N samples is $X = \{x_1, x_2, \ldots, x_N\}$, the PDF of which is expressed in (1), then the log-likelihood function of X can be expressed as:

$$\ln[L(\Theta|X)] = \ln\left[\prod_{i=1}^{N} p(x_i|\Theta)\right]$$
$$= \sum_{i=1}^{N} \ln[p(x_i|\Theta)] = \sum_{i=1}^{N} \ln\left[\sum_{k=1}^{M} \omega_k p_k(x_i|\theta_k)\right] \quad (16)$$

The essence of the EM algorithm is to find the value of Θ that maximizes $L(\Theta|X)$. However, (16) includes additions in logarithm, so it is not feasible to directly calculate the extreme

value directly by derivation. To simplify the likelihood function expression, a set of random variable $Y = \{y_1, y_2, \cdots, y_N\}$ is introduced, and $y_i \in \{1, 2, \cdots, M\}$, $i = 1, 2, \ldots, N$, $y_i = k$ indicates that the i-th sample x_i is generated by the k-th Gaussian distribution.

Then, the log-likelihood function of the complete data can be expressed as:

$$\ln[L(\Theta|X, Y)] = \ln\left[\prod_{i=1}^{N} p(x_i, y_i|\Theta)\right]$$
$$= \sum_{i=1}^{N} \ln[p(y_i|\theta_{y_i}) p(x_i|y_i, \theta_{y_i})]$$
$$= \sum_{i=1}^{N} \ln[\omega_{y_i} p_{y_i}(x_i|\theta_{y_i})] \quad (17)$$

The EM algorithm can be summarized in 3 steps:

1) E-Step: Calculate the log-likelihood function expectation of the complete data $Q(\Theta|\Theta^{(t)})$;

2) M-Step: Calculate the parameter $\Theta^{(t+1)}$ that maximizes $Q(\Theta|\Theta^{(t)})$;

3) Perform E-Step and M-Step alternately until convergence.

The detailed process is as follows:

1) E-Step: Suppose that at the beginning of the t-th iteration, the estimated value of Θ is $\Theta^{(t)} = (\omega_1^{(t)}, \omega_2^{(t)}, \ldots, \omega_M^{(t)}, \theta_1^{(t)}, \theta_2^{(t)}, \ldots, \theta_M^{(t)})$, then, the expectation of the log-likelihood function of the complete data becomes:

$$Q\left(\Theta|\Theta^{(t)}\right)$$
$$= E\left\{\ln[L(\Theta|X, Y)]|X, \Theta^{(t)}\right\}$$
$$= \int_{y \in D} \ln[L(\Theta|X, y)] p\left(y|X, \Theta^{(t)}\right) dy$$
$$= \int_{y \in D} \sum_{i=1}^{N} \ln[\omega_{y_i} p_{y_i}(x_i|\theta_{y_i})] p\left(y|x_i, \Theta^{(t)}\right) dy \quad (18)$$

where D is the value space of y.

Assuming the probability that the i-th sample x_i is generated by the k-th Gaussian distribution be $p(y_i = k|x_i, \Theta^{(t)})$, then (18) becomes:

$$Q\left(\Theta|\Theta^{(t)}\right)$$
$$= \sum_{k=1}^{M} \sum_{i=1}^{N} \ln[\omega_k p_k(x_i|\theta_k)] p\left(k|x_i, \Theta^{(t)}\right)$$
$$= \sum_{k=1}^{M} \sum_{i=1}^{N} \ln(\omega_k) p\left(k|x_i, \Theta^{(t)}\right)$$
$$+ \sum_{k=1}^{M} \sum_{i=1}^{N} \ln[p_k(x_i|\theta_k)] p\left(k|x_i, \Theta^{(t)}\right) \quad (19)$$

TABLE 13. Log-normal distribution parameters of driving time in minutes.

Trip day	Departure	Destination					
		Home	Work	Shopping	Entertainment	Pick-up	Dining
Weekday (μ_v, σ_v)	Home	(2.42, 0.74)	(2.17, 0.84)	(2.57, 0.82)	(3.14, 0.93)	(2.42, 0.85)	(2.29, 0.93)
	Work	(2.84, 1.02)	(2.35, 0.76)	(2.93, 0.74)	(2.79, 0.84)	(2.37, 0.78)	(2.44, 0.77)
	Shopping	(3.00, 0.77)	(2.72, 0.83)	(2.77, 0.95)	(2.96, 0.85)	(2.84, 0.80)	(2.35, 0.77)
	Entertainment	(2.82, 0.83)	(2.77, 0.92)	(2.43, 0.89)	(2.81, 0.94)	(2.94, 0.86)	(2.55, 0.81)
	Pick-up	(2.39, 0.77)	(2.44, 0.81)	(2.71, 0.82)	(2.97, 0.87)	(2.34, 0.82)	(2.41, 0.77)
	Dining	(2.54, 0.76)	(2.36, 0.95)	(2.31, 0.75)	(2.86, 1.03)	(2.58, 0.86)	(2.46, 0.97)
Weekend (μ_v, σ_v)	Home	(2.43, 0.74)	(2.16, 0.87)	(2.38, 0.80)	(2.94, 0.92)	(2.55, 0.79)	(2.46, 1.03)
	Work	(2.91, 1.11)	(2.40, 0.74)	(2.73, 0.79)	(2.96, 0.83)	(2.56, 0.87)	(2.57, 0.82)
	Shopping	(2.84, 0.79)	(2.46, 0.83)	(2.75, 0.95)	(2.71, 0.73)	(2.82, 0.79)	(2.45, 0.75)
	Entertainment	(2.98, 0.85)	(2.82, 0.94)	(2.70, 0.85)	(3.11, 1.05)	(2.99, 1.15)	(2.83, 0.89)
	Pick-up	(2.56, 0.90)	(2.67, 1.05)	(2.86, 0.81)	(3.11, 0.87)	(2.68, 0.91)	(2.59, 0.86)
	Dining	(2.61, 0.84)	(2.46, 0.91)	(2.25, 0.87)	(2.77, 0.93)	(2.81, 0.92)	(2.57, 1.07)

Base on Bayesian theory, the posterior probability $p(k| x_i, \Theta^{(t)})$ in (19) can be expressed as

$$p\left(k|x_i, \Theta^{(t)}\right) = \frac{p\left(k, x_i|\theta_k^{(t)}\right)}{p\left(x_i|\Theta^{(t)}\right)} = \frac{\omega_k p_k\left(x_i|\theta_k^{(t)}\right)}{\sum_{j=1}^{M} \omega_j p_j\left(x_i|\theta_j^{(t)}\right)} \quad (20)$$

2) M-Step: Calculate the parameter $\Theta^{(t+1)}$ that maximizes $Q(\Theta|\Theta^{(t)})$.

a) Calculation for $\omega_k^{(t+1)}$. Introduce Lagrange multiplier λ into $Q(\Theta|\Theta^{(t)})$, and let the partial derivative of $Q(\Theta|\Theta^{(t)})$ to ω_k be 0:

$$\frac{\partial}{\partial \omega_k}\left[Q\left(\Theta|\Theta^{(t)}\right) + \lambda\left(\sum_{k=1}^{M} \omega_k - 1\right)\right]$$

$$= \frac{\partial}{\partial \omega_k}\left[\sum_{k=1}^{M}\sum_{i=1}^{N} \ln(\omega_k)p\left(k|x_i, \Theta^{(t)}\right) + \lambda\left(\sum_{k=1}^{M} \omega_k - 1\right)\right] + 0$$

$$= \frac{1}{\omega_k}\sum_{i=1}^{N} Mp\left(k|x_i, \Theta^{(t)}\right) + \lambda M$$

$$= 0 \quad (21)$$

Then, the following results can be derived:

$$\sum_{i=1}^{N} p\left(k|x_i, \Theta^{(t)}\right) + \lambda \omega_k = 0 \quad (22)$$

Sum k on both sides of (22):

$$\begin{cases} \sum_{k=1}^{M}\left[\sum_{i=1}^{N} p\left(k|x_i, \Theta^{(t)}\right) + \lambda \omega_k\right] = 0 \\ \sum_{k=1}^{M} p\left(k|x_i, \Theta^{(t)}\right) = 1 \\ \sum_{k=1}^{M} \omega_k = 1 \end{cases} \quad (23)$$

Then, it can be derived that $\lambda = -N$. Substituting it into (22), the following result can be obtained:

$$\omega_k^{(t+1)} = \frac{\sum_{i=1}^{N} p\left(k|x_i, \Theta^{(t)}\right)}{N} \quad (24)$$

b) Calculation for $\mu_k^{(t+1)}$. Assuming the partial derivative of $Q(\Theta|\Theta^{(t)})$ to μ_k is 0:

$$\frac{\partial Q\left(\Theta|\Theta^{(t)}\right)}{\partial \mu_k}$$

$$= 0 + \frac{\partial}{\partial \mu_k}\left[\sum_{k=1}^{M}\sum_{i=1}^{N} \ln[p_k(x_i|\theta_k)]p\left(k|x_i, \Theta^{(t)}\right)\right]$$

$$= \frac{\partial}{\partial \mu_k}\left[\sum_{i=1}^{N}\left[\ln\left(\sqrt{2\pi\sigma_k^2}\right)^{-1} - \frac{(x_i-\mu_k)^2}{2\sigma_k^2}\right]p\left(k|x_i, \Theta^{(t)}\right)\right]$$

$$= \frac{1}{\sigma_k^2}\sum_{i=1}^{N}\left[x_i p\left(k|x_i, \Theta^{(t)}\right)\right] - \frac{\mu_k}{\sigma_k^2}\sum_{i=1}^{N} p\left(k|x_i, \Theta^{(t)}\right)$$

$$= 0 \quad (25)$$

Then:

$$\mu_k^{(t+1)} = \frac{\sum_{i=1}^{N}\left[x_i p\left(k|x_i, \Theta^{(t)}\right)\right]}{\sum_{i=1}^{N} p\left(k|x_i, \Theta^{(t)}\right)} \quad (26)$$

c) Calculation for $\sigma_k^{(t+1)}$. Similarly, assuming the partial derivative of $Q(\Theta|\Theta^{(t)})$ to $(\sigma_k^2)^{-1}$ be 0:

$$\frac{\partial Q\left(\Theta|\Theta^{(t)}\right)}{\partial\left(\sigma_k^{-2}\right)}$$

$$= 0 + \frac{\partial}{\partial\left(\sigma_k^{-2}\right)}\left[\sum_{k=1}^{M}\sum_{i=1}^{N} \ln[p_k(x_i|\theta_k)]p\left(k|x_i, \Theta^{(t)}\right)\right]$$

$$= \frac{\partial}{\partial\left(\sigma_k^{-2}\right)}\left[\sum_{i=1}^{N}\left[\ln\left(\sqrt{2\pi\sigma_k^2}\right)^{-1} - \frac{(x_i-\mu_k)^2}{2\sigma_k^2}\right]p\left(k|x_i, \Theta^{(t)}\right)\right]$$

$$= \sum_{i=1}^{N}\left[\frac{1}{2\sigma_k^{-2}} - \frac{(x_i - \mu_k)^2}{2}\right]p\left(k|x_i, \Theta^{(t)}\right)$$

$$= 0 \quad (27)$$

Then:

$$\left(\sigma_k^2\right)^{(t+1)} = \frac{\sum_{i=1}^{N}\left[(x_i - \mu_k)^2 p\left(k|x_i, \Theta^{(t)}\right)\right]}{\sum_{i=1}^{N}\left[p\left(k|x_i, \Theta^{(t)}\right)\right]} \quad (28)$$

3) Perform E-Step and M-Step alternately until convergence:

$$\max \left(\left| \omega_k^{(t+1)} - \omega_k^{(t)} \right|, \left| \mu_k^{(t+1)} - \mu_k^{(t)} \right|, \left| \sigma_k^{(t+1)} - \sigma_k^{(t)} \right| \right) < \varepsilon$$
$$, \forall k \in \{1, 2, \cdots, M\} \qquad (29)$$

where ε is the error threshold.

APPENDIX B
LOG-NORMAL DISTRIBUTION PARAMETERS OF DRIVING TIME IN MINUTES
See Table 13.

REFERENCES

[1] F. Zhang, Z. Hu, X. Xie, J. Zhang, and Y. Song, "Assessment of the effectiveness of energy storage resources in the frequency regulation of a single-area power system," *IEEE Trans. Power Syst.*, vol. 32, no. 5, pp. 3373–3380, Sep. 2017.

[2] H. Liu, J. Qi, J. Wang, P. Li, C. Li, and H. Wei, "EV dispatch control for supplementary frequency regulation considering the expectation of EV owners," *IEEE Trans. Smart Grid*, vol. 9, no. 4, pp. 3763–3772, Jul. 2018.

[3] P. Yang, X. Dong, Y. Li, L. Kuang, J. Zhang, B. He, and Y. Wang, "Research on primary frequency regulation control strategy of wind-thermal power coordination," *IEEE Access*, vol. 7, pp. 144766–144776, 2019.

[4] Y. Sun, H. Yue, J. Zhang, and C. Booth, "Minimization of residential energy cost considering energy storage system and EV with driving usage probabilities," *IEEE Trans. Sustain. Energy*, vol. 10, no. 4, pp. 1752–1763, Oct. 2019.

[5] J. Zhao, J. Wang, Z. Xu, C. Wang, C. Wan, and C. Chen, "Distribution network electric vehicle hosting capacity maximization: A chargeable region optimization model," *IEEE Trans. Power Syst.*, vol. 32, no. 5, pp. 4119–4130, Sep. 2017.

[6] J. Wang, G. R. Bharati, S. Paudyal, O. Ceylan, B. P. Bhattarai, and K. S. Myers, "Coordinated electric vehicle charging with reactive power support to distribution grids," *IEEE Trans. Ind. Informat.*, vol. 15, no. 1, pp. 54–63, Jan. 2019.

[7] K. R. Reddy and S. Meikandasivam, "Load flattening and voltage regulation using plug-in electric vehicle's storage capacity with vehicle prioritization using ANFIS," *IEEE Trans. Sustain. Energy*, vol. 11, no. 1, pp. 260–270, Jan. 2020.

[8] Y. Zheng, Y. Song, D. J. Hill, and K. Meng, "Online distributed MPC-based optimal scheduling for EV charging stations in distribution systems," *IEEE Trans. Ind. Informat.*, vol. 15, no. 2, pp. 638–649, Feb. 2019.

[9] L. Calearo, A. Thingvad, K. Suzuki, and M. Marinelli, "Grid loading due to EV charging profiles based on pseudo-real driving pattern and user behavior," *IEEE Trans. Transport. Electrific.*, vol. 5, no. 3, pp. 683–694, Sep. 2019.

[10] O. Hafez and K. Bhattacharya, "Integrating EV charging stations as smart loads for demand response provisions in distribution systems," *IEEE Trans. Smart Grid*, vol. 9, no. 2, pp. 1096–1106, Mar. 2018.

[11] H. Yuan, G. Wei, L. Zhu, X. Zhang, H. Zhang, Z. Luo, and J. Hu, "Optimal scheduling for micro-grid considering EV charging–swapping–storage integrated station," *IET Gener., Transmiss. Distrib.*, vol. 14, no. 6, pp. 1127–1137, Mar. 2020.

[12] K. Chaudhari, N. K. Kandasamy, A. Krishnan, A. Ukil, and H. B. Gooi, "Agent-based aggregated behavior modeling for electric vehicle charging load," *IEEE Trans. Ind. Informat.*, vol. 15, no. 2, pp. 856–868, Feb. 2019.

[13] W. Yang, Y. Xiang, J. Liu, and C. Gu, "Agent-based modeling for scale evolution of plug-in electric vehicles and charging demand," *IEEE Trans. Power Syst.*, vol. 33, no. 2, pp. 1915–1925, Mar. 2018.

[14] J. Rolink and C. Rehtanz, "Large-scale modeling of grid-connected electric vehicles," *IEEE Trans. Power Del.*, vol. 28, no. 2, pp. 894–902, Apr. 2013.

[15] D. Tang and P. Wang, "Probabilistic modeling of nodal charging demand based on spatial-temporal dynamics of moving electric vehicles," *IEEE Trans. Smart Grid*, vol. 7, no. 2, pp. 627–636, Mar. 2015.

[16] Q. Zhang, Y. Zhu, Z. Wang, Y. Su, and C. Li, "Reliability assessment of distribution network and electric vehicle considering quasi-dynamic traffic flow and vehicle-to-grid," *IEEE Access*, vol. 7, pp. 131201–131213, 2019.

[17] T. Shun, W. Jianfeng, X. Xiangning, Z. Jian, L. Kunyu, and Y. Yang, "Charging demand for electric vehicle based on stochastic analysis of trip chain," *IET Gener., Transmiss. Distrib.*, vol. 10, no. 11, pp. 2689–2698, Aug. 2016.

[18] E. B. Iversen, J. K. Moller, J. M. Morales, and H. Madsen, "Inhomogeneous Markov models for describing driving patterns," *IEEE Trans. Smart Grid*, vol. 8, no. 2, pp. 581–588, Mar. 2016.

[19] D. Xie, H. Chu, C. Gu, F. Li, and Y. Zhang, "A novel dispatching control strategy for EVs intelligent integrated stations," *IEEE Trans. Smart Grid*, vol. 8, no. 2, pp. 802–811, Aug. 2015.

[20] E. Yao, V. W. S. Wong, and R. Schober, "Robust frequency regulation capacity scheduling algorithm for electric vehicles," *IEEE Trans. Smart Grid*, vol. 8, no. 2, pp. 984–997, Mar. 2017.

[21] K. Kaur, N. Kumar, and M. Singh, "Coordinated power control of electric vehicles for grid frequency support: MILP-based hierarchical control design," *IEEE Trans. Smart Grid*, vol. 10, no. 3, pp. 3364–3373, May 2019.

[22] G. Buja, M. Bertoluzzo, and C. Fontana, "Reactive power compensation capabilities of V2G-enabled electric vehicles," *IEEE Trans. Power Electron.*, vol. 32, no. 12, pp. 9447–9459, Dec. 2017.

[23] G. Wenzel, M. Negrete-Pincetic, D. E. Olivares, J. MacDonald, and D. S. Callaway, "Real-time charging strategies for an electric vehicle aggregator to provide ancillary services," *IEEE Trans. Smart Grid*, vol. 9, no. 5, pp. 5141–5151, Sep. 2018.

[24] S. Li, J. Li, C. Su, and Q. Yang, "Optimization of bi-directional V2G behavior with active battery anti-aging scheduling," *IEEE Access*, vol. 8, pp. 11186–11196, 2020.

[25] X. Wang and Q. Liang, "Energy management strategy for plug-in hybrid electric vehicles via bidirectional vehicle-to-grid," *IEEE Syst. J.*, vol. 11, no. 3, pp. 1789–1798, Sep. 2017.

[26] A. Ravichandran, S. Sirouspour, P. Malysz, and A. Emadi, "A chance-constraints-based control strategy for microgrids with energy storage and integrated electric vehicles," *IEEE Trans. Smart Grid*, vol. 9, no. 1, pp. 346–359, Jan. 2018.

[27] X. Dou, X. Duan, Q. Hu, L. Shen, and Z. Wu, "A nonintrusive control strategy using voltage and reactive power for distribution systems based on PV and the nine-zone diagram," *Int. J. Electr. Power Energy Syst.*, vol. 105, pp. 89–97, Feb. 2019.

[28] Z. Qiang, Z. Zhengdao, J. Yingjun, L. Jianhan, and L. Yong, "Research on reactive voltage control strategy of substations based on space nine-domain diagram," in *Proc. 13th IEEE Conf. Ind. Electron. Appl. (ICIEA)*, Jun. 2018, pp. 1627–1632.

[29] N. S. Daisy, L. Liu, and H. Millward, "Trip chaining propensity and tour mode choice of out-of-home workers: Evidence from a mid-sized Canadian city," *Transportation*, vol. 47, no. 2, pp. 763–792, Apr. 2020.

[30] Y. Xiang, Z. Jiang, C. Gu, F. Teng, X. Wei, and Y. Wang, "Electric vehicle charging in smart grid: A spatial-temporal simulation method," *Energy*, vol. 189, Dec. 2019, Art. no. 116221.

[31] D. Fischer, A. Harbrecht, A. Surmann, and R. McKenna, "Electric vehicles' impacts on residential electric local profiles—A stochastic modelling approach considering socio-economic, behavioural and spatial factors," *Appl. Energy*, vols. 233–234, pp. 644–658, Jan. 2019.

[32] A. P. Dempster, N. M. Laird, and D. B. Rubin, "Maximum likelihood from incomplete data via the EM algorithm," *J. Roy. Stat. Soc. B, Methodol.*, vol. 39, no. 1, pp. 1–38, 1977.

[33] Global and U.S. Electric Vehicle Trends. *International Council on Clean Transportation (ICCT)*. Accessed: Apr. 25, 2020. [Online]. Available: https://theicct.org/sites/default/files/Drew%20Kodjak_Canada%20global%20EV_12June2019_0.pdf

[34] U.S. Department of Energy. *AVTA: ARRA EV Project Nissan Leaf Data Summary Reports*. Accessed: Apr. 25, 2020. [Online]. Available: https://www.energy.gov/eere/vehicles/downloads/avta-arra-ev-project-nissan-leaf-data-summary-reports

[35] N. S. Sains and I. Al-Anbagi, "Optimal charging and discharging for EVs in a V2G participation under critical peak conditions," *IET Electr. Syst. Transp.*, vol. 8, no. 2, pp. 136–143, Dec. 2017.

[36] C. Liu, K. K. Chai, X. Zhang, E. T. Lau, and Y. Chen, "Adaptive blockchain-based electric vehicle participation scheme in smart grid platform," *IEEE Access*, vol. 6, pp. 25657–25665, 2018.

[37] T. Mao, W.-H. Lau, C. Shum, H. S.-H. Chung, K.-F. Tsang, and N. C.-F. Tse, "A regulation policy of EV discharging price for demand scheduling," *IEEE Trans. Power Syst.*, vol. 33, no. 2, pp. 1275–1288, Mar. 2018.

[38] X. Wang, C. Sun, R. Wang, and T. Wei, "Two-stage optimal scheduling strategy for large-scale electric vehicles," *IEEE Access*, vol. 8, pp. 13821–13832, 2020.

[39] Z. Luo, Z. Hu, Y. Song, X. Yang, K. Zhan, and J. Wu, "Study on plug-in electric vehicles charging load calculating," *Autom. Electr. Power Syst.*, vol. 35, no. 14, pp. 36–42, 2011.

[40] H. S. Chwa, J. Lee, J. Lee, K.-M. Phan, A. Easwaran, and I. Shin, "Global EDF schedulability analysis for parallel tasks on multi-core platforms," *IEEE Trans. Parallel Distrib. Syst.*, vol. 28, no. 5, pp. 1331–1345, May 2017.

[41] G. Kan, T. Lei, K. Liang, J. Li, L. Ding, X. He, H. Yu, D. Zhang, D. Zuo, Z. Bao, M. Amo-Boateng, Y. Hu, and M. Zhang, "A multi-core CPU and many-core GPU based fast parallel shuffled complex evolution global optimization approach," *IEEE Trans. Parallel Distrib. Syst.*, vol. 28, no. 2, pp. 332–344, Feb. 2017.

[42] A. Bhuiyan, D. Liu, A. Khan, A. Saifullah, N. Guan, and Z. Guo, "Energy-efficient parallel real-time scheduling on clustered multi-core," *IEEE Trans. Parallel Distrib. Syst.*, vol. 31, no. 9, pp. 2097–2111, Sep. 2020.

[43] Amazon. *Amazon Web Services (AWS)—Cloud Computing Services.* Accessed: Jun. 1, 2020. [Online]. Available: https://aws.amazon.com/

[44] Microsoft. *Microsoft Azure: Cloud Computing Services.* Accessed: Jun. 1, 2020. [Online]. Available: https://azure.microsoft.com/

[45] HUAWEI. *HUAWEI CLOUD-Grow With Intelligence.* Accessed: Jun. 1, 2020. [Online]. Available: https://www.huaweicloud.com/

HAIFENG LIANG (Member, IEEE) was born in China, in 1976. He received the B.S. and Ph.D. degrees from North China Electric Power University (NCEPU), in 1998 and 2009, respectively, and the M.S. degree from the Huazhong University of Science and Technology, 2001.

He was a Visiting Scholar with Cardiff University, Cardiff, U.K., in 2016. Since 2001, he has been with the Department of Electrical Engineering, NCEPU. He is currently an Associate Professor. His research interests include new transmission and distribution technologies, micro-grid, and distributed generation and its grid integration technologies.

ZIYANG LEE was born in China, in 1996. He received the B.E. degree in electrical engineering from Yanshan University, Qinhuangdao, China, in 2018. He is currently pursuing the M.Sc. degree with the Department of Electrical Engineering, North China Electric Power University, Baoding, China.

His research interests include V2G, smart grids, machine learning, and renewable power generation optimal dispatch.

GEN LI (Member, IEEE) received the B.Eng. degree in electrical engineering and its automation from Northeast Electric Power University, Jilin, China, in 2011, the M.Sc. degree in power engineering from Nanyang Technological University, Singapore, in 2013, and the Ph.D. degree in electrical engineering from Cardiff University, Cardiff, U.K., in 2018.

From 2013 to 2016, he was a Marie Curie Early Stage Research Fellow funded by the European Union's MEDOW Project. He has been a Visiting Researcher with the China Electric Power Research Institute and the Global Energy Interconnection Research Institute, Beijing, China, at Elia, Brussels, Belgium, and at Toshiba International, Europe, London, U.K. He has been a Research Associate with the School of Engineering, Cardiff University, since 2017. His research interests include control and protection of HVDC and MVDC technologies, power electronics, reliability modeling, and evaluation of power electronics systems.

Dr. Li is an Editorial Board Member of CIGRE ELECTRA. He is a Chartered Engineer in the U.K. He is an Associate Editor of the *CSEE Journal of Power and Energy Systems*. His Ph.D. thesis received the First CIGRE Thesis Award, in 2018.

・・・